Chapter 12
Organic Rankine Cycles (ORCs) for Waste Heat Utilization

Yong-qiang Feng and Tzu-Chen Hung

Abstract Considering the thermodynamic performance, economic performance, and environmental performance simultaneously, the thermo-environmental optimization for a series dual-pressure organic Rankine cycle (STORC) and a cascaded organic Rankine cycle (CORC) has been investigated. The effects of key operating parameters on the thermal and economic performance of the system were analyzed. Based on a 3 kW ORC experimental prototype, the heat exchanger performance of different mixtures has been studied and compared. Five different proportions of working fluids were selected, respectively, R123, 0.33R123/0.67R245fa, 0.5R123/0.5R245fa, 0.67R123/0.33R245fa, and R245fa. The comparison between the experimental test and simulation result without considering the pressure drop was addressed. Results indicate that R245fa/R152a is the best candidate working fluids for CORC LT-Loop. The evaporator heat transfer coefficients of R245fa are highest, followed by the R245fa/R123 mixture and while R123 shows the lowest evaporator heat coefficients. The measured thermal efficiency of 0.67R123/0.33R245fa is the highest, which is 7.33% and the maximum simulated thermal efficiency is14.55%.

Keywords Organic Rankine cycle (ORC) · Thermo-environmental optimization · Evaporator heat coefficient · Pressure drop

12.1 Introduction

At the current energy consumption rate and population growth rate, the world's proven reserves of coal can last up to 200 years, and oil and natural gas can last up to 50 years. Building a clean, safe, low-carbon, and efficient modern energy system is an important way to achieve high-quality urban energy development. With

Y. Feng (✉)
School of Energy and Power Engineering, Jiangsu University, Zhenjiang, China
e-mail: yqfeng@ujs.edu.cn

T.-C. Hung
Department of Mechanical Engineering, National Taipei University of Technology, Taipei, Taiwan
e-mail: tchung@ntut.edu.tw

© The Author(s), under exclusive license to Springer Nature Switzerland AG 2022

A. E.-F. Abomohra et al. (eds.), *Waste-to-Energy*,
https://doi.org/10.1007/978-3-030-91570-4_12

the development of economy, urbanization rate increase, the production and living energy consumption is also growing, but the total energy is limited, environmental capacity is limited, and how to maintain the continuous growth of the industrial economy and the continuous improvement of people's living standards and to control the total energy consumption and improve energy utilization efficiency become the problem that needs to solve. So based on the present situation of the traditional fossil energy at a time and the burning of fossil fuels at a time using great pollution to the environment after the two main aspects, the world health organization and various countries work together to develop a variety of the constraints of energy-saving and emission reduction policy, such as developing renewable energy, upgrading system equipment and product innovation, and the recycle of energy strategy. However, the recycling and utilization of energy have been paid more and more attention by human beings, because the utilization efficiency of heat of combustion is limited. In general, the utilization efficiency of heat of combustion does not exceed 50% of the heat generated by combustion, and the part of heat not used by combustion is lost and wasted in vain. The global energy efficiency is low, an important reason is that more than a large amount of waste heat pressure is not fully achieve cascade utilization of resources, the key factors to restrict energy efficiency of energy-saving technology is backward, and there are many types of use of waste heat recovery technology; main technologies are heat exchange technology, cooling, heating, and thermal power generation technology, and because the structure of the heat exchange and thermal conversion technology is relatively single, and the application range is smaller, the recovery efficiency is low, so we chose thermal power generation technology for key research. Thermal power generation technology is mainly based on the thermal power generation system of Rankine cycle, like the organic Rankine cycle (ORC), Kalina cycle, water vapor expansion cycle, etc. However, ORC is the most widely studied and applied. ORC is a circulation system with low boiling point organic matter as the working medium, which can recover low-temperature thermal energy of different temperature gradients and has a high efficiency in sensible heat recovery (Zhou et al. 2013; Yamada et al. 2014).

Under one atmosphere, some organic working fluids have lower boiling points, so the lower heat absorption can be evaporated to form a higher pressure. According to these characteristics of organic working fluid with a lower boiling point, the L–T (low temperature) heat source can be used to heat it to produce high-pressure (H-P) gas, and the expander can be pushed to do work to realize the recovery and utilization of L–T heat energy. Compared with water, organic working fluid has strong superiority, an ORC system the working fluid of choice is proper, can improve the system efficiency and output power, choose the ORC system cycle working substance to the heat source temperature, evaporation temperature, evaporation pressure, condensation temperature and the pinch point temperature difference and so on carries on the comprehensive consideration, for the characteristics of different fluid to domestic and foreign scholars have conducted a long-term research. Tian et al. (2012, 2014, 2017; Song and Gu 2015) used R134a and R245fa as working medium and used experimental methods to compare the organic Rankine cycle system with flue gas as heat source at 400 °C. The comprehensive comparison found that R134a had

better performance in the L–T section, while R245fa had better performance in the H-T (high-temperature) section. Shu et al. (2016) adopted regenerative organic Rankine cycle system and selected five working fluids, R134a, R245fa, pentane, MDM and toluene, to analyze the influence of key parameters on the thermodynamic performance of the system. It is found that the cycle efficiency can be improved by increasing evaporation pressure, evaporation temperature, and expansion ratio, but the superheat has little effect on the cycle performance. Dong et al. (2017) taken R245fa as working fluid, although the calculation model can be simplified for only one type of working fluid, due to the limitations of each type of working fluid, the pure working fluid may not achieve the best effect. For some circulatory systems, mixed working media are more advantageous. Wang et al. (2018) compared the coupling ORC system with single stage across critical ORC system performance and probe into the critical temperature and the working medium combination working medium influence on coupling ORC system performance. Uusitalo et al. (2014) studied a coupling across the critical and subcritical organic Rankine's circulatory system and performance analysis of the coupling ORC system in detail. Javanshir et al. (2017) proposed the ejector organic Rankine cycle and carried out thermodynamic studies on the ejector organic Rankine cycle under subcritical, transcritical, and supercritical conditions. Lim et al. (2021) evaluated the system with nine groups of mixed refrigerants, and the results showed that R123-R245fa had the highest net power. Zhang et al. (2021a) used 36 kinds of working fluids and determined the type of pump suitable for working fluids, which provided reference for practical operation.

In addition to changing the choice of working medium, the thermal efficiency of the system can be improved by optimizing the structural parameters of the system. Wang et al. (2020a) optimized and compared the single-stage evaporation and two-stage evaporation organic Rankine cycles and found that the latter has the smallest generation cost and investment payback period. Kim et al. (2020) proposed a system combining phosphoric acid fuel cell (PAFC) and organic Rankine cycle, and the thermal efficiency increased by 11.31%. Esra and Kiliç (2020) combined ORC with VCRC, and the exergy efficiency of the system was increased by 19.5%. Renno et al. (2020) proposed a new ORC system (CPV/T). Compared with the original ORC, the system efficiency was improved by 2.6%. Zhang et al. (2021b) proposed a new ICE-ORC system for different rated power of ICE, and compared with the traditional system, the cycle efficiency was improved by 17%. Kang et al. (2020) analyzed the performance of ORC systems combined with other circulatory systems and found that the power generation could be increased by up to 20%. Huang et al. (2019) added ORC equipment on the basis of CCHP. Through data comparison, they found that all indexes of CCHP-ORC system were superior to the original system. Shu et al. (2014a) conducted a CORC to recover various waste heat and found that R1234yf was the best working fluid.

In addition, many teams have presented interests in the mixed working fluid. Shu et al. (2020) investigated the dynamic performance of cascade system by dynamic simulation. Results show that the cascade systems are better than other systems in terms of waste heat utilization. Shu et al. (2014b) investigated the thermal efficiency for ORC system used two retardants. The results revealed that in comparison with pure working fluids, zeotropic mixtures presented a more satisfactory thermodynamic performance. The similar conclusion can be found by Heberle et al. (2012) and Zhang et al. (2014). Lecompte et al. (2014) examined the exergy efficiency on ORC system used mixed working fluid. The results showed that the thermal efficiency of mixed medium is higher than that of pure medium. Dong et al. (2014) studied the first law thermal efficiency on ORC system used mixed working fluid. Feng et al. (2015a) compared the thermodynamic properties of pure working medium and mixed working medium, and found that the mixed working fluid had low thermodynamic properties. In their subsequent study (Feng et al. 2015b), a thermo-economical compassion considering exergy efficiency and leveled energy cost (LEC) simultaneously was examined. The results indicated that the zeotropic working fluids do not always have more advantageous than pure working fluids. The similar conclusion can be found in Xiao et al. (2015), and studies have shown that the composite properties of mixed working fluids are sometimes not as good as those of pure working fluids. The above reference demonstrates that the mixture working fluids represented better thermodynamic performance and economic performance than the pure working fluid at certain heat source condition and mass fraction. Tian et al. (Wang et al. 2020b) proposed dual-loop ORC system which uses zeotropic mixtures based on siloxanes. Results indicated that D4/R123 (0.3/0.7) has best performance with net-power output of 21.66 kW and the thermal efficiency of 22.84%. Aziz et al. (2018) optimized the H-T organic Rankine cycle by genetic algorithm, and the UA value of decane increased by 45.5%. Wang et al. (2020c) used genetic algorithm for multi-objective optimization of ORC and sorted the Pareto optimal solution to obtain the optimal operation parameters. Imran et al. (2016) evaluated three different orcs and compared them by genetic algorithm. It was found that the thermal efficiency and exergy efficiency of RORC were higher than ORC, but the average investment cost was higher. Li and Li (2018a) carried out two objective optimization on SORC, and further analyzed the influence of different parameter combinations in Pareto boundary and SORC scale on economic performance.

In this chapter, the thermo-environmental optimization for a series dual-pressure organic Rankine cycle (STORC) and a cascaded organic Rankine cycle (CORC) has been researched. The effects of key parameters on the thermal and economic performance of the system were analyzed. Based on a 3 kW ORC experimental prototype, the heat exchanger performance of different mixtures has been studied and compared. Five different proportions of working fluids were selected, respectively, R123, 0.33R123/0.67R245fa, 0.5R123/0.5R245fa, 0.67R123/0.33R245fa, and R245fa. The comparison between the experimental test and simulation result without considering the pressure drop was addressed.

12.2 Thermo-environmental Optimization of a Novel Supercritical–Subcritical Organic Rankine Cycle

12.2.1 System Description of STORC

Figure 12.1 shows the STORC system flowchart, which mainly includes a H-P evaporator, a L-P (low pressure) evaporator, a preheater, a condenser, and two expanders. The T-s diagram of the STORC system is shown in Fig. 12.2. The working fluid is preheated by the preheater (process 2–3) and divided into two parts, and the first part flows into the H-P cycle, while the remaining working fluid flows into the L-P cycle. The working fluid is further pressurized by a H-P pump to a higher evaporative pressure (process 3–5), and then vaporized to saturation or overheating by absorbing heat from the heat source (process 5–8). The working fluid with H-T and H-P flows into the H-P expander, and output work is done (process 8–9). The remaining working fluid is heated by the L-P evaporator until it is saturated or overheated (process 3–10). The working fluid from the H-P expander (point 9) mixes with the one from the L-P evaporator (point 10) and then flows into the L-P expander to generate work output (process 11–12). The working fluid is then condensed through the condenser (process 12–1) and then fed into the working pump for the next cycle. It should be noted that the H-P and L-P loop are subcritical ORC cycle, while the mixture working fluid is adopted in this study.

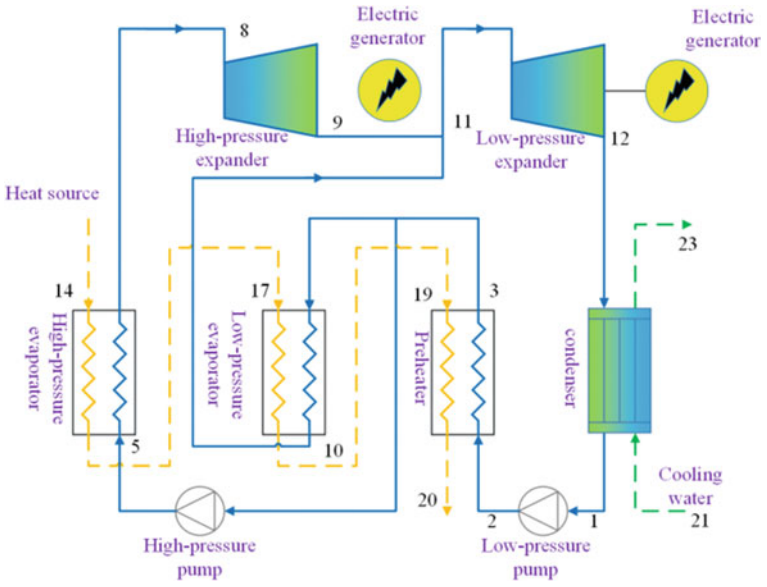

Fig. 12.1 Schematic of the STORC system

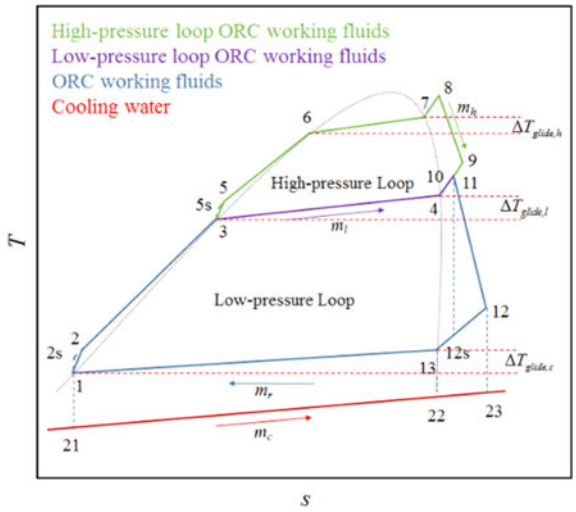

Fig. 12.2 T-s diagram of the STORC system

12.2.2 Analysis of STORC Operating Parameters

12.2.2.1 Parametric Analysis

The hot and cold sources in this article remain the same as in the second chapter. For related parameters, please refer to the second chapter. From the above STORC system's flowchart and temperature entropy chart, it can be found that mixed working fluid components, H-P evaporator inlet temperature, L-P evaporator inlet temperature, condensation temperature, superheat, and pinch point temperature difference have important effects on the system's performance. This section analyzes the impact of these six operating parameters on the system's performance. In this section, R245fa, pentane, and their mixtures are chosen as working fluids for the STORC. R245fa and pentane have good thermal properties. Table 12.1 shows the basic parameters of the STORC system. The bubble and dew point positions of the evaporator and condenser influence the comparison of the system's performance under mixed working fluid and pure working fluid. In this paper, the saturated liquid phase point is set to correspond to the evaporation temperature or condensation temperature.

12.2.2.2 Influence of H-P Circulation Evaporation Temperature on System Performance

The change of system's efficiency with the H-T cycle evaporation temperature is shown in Fig. 12.3. The results showed that the tritium efficiency of the three working media showed the same trend. The specific analysis shows that when the H-T circulation evaporation temperature rises, the pinch point of the H-P evaporator moves

Table 12.1 Initial operating parameter of the STORC system

Parameters	Symbol	Value
Heat mass flow (kg/s)	$\dot{m}_g$	1
Heat inlet temperature (K)	$T_{g,\text{in}}$	423
Heat stress (kPa)	P_g	101.325
Cooling water inlet temperature (K)	$T_{\text{c,in}}$	288
Cooling water pressure (kPa)	P_c	101.325
The narrow temperature difference in H-P evaporator (K)	$\Delta T_{\text{pp,h}}$	3–10
The pinch point temperature difference between L-P evaporator (K)	$\Delta T_{\text{pp,l}}$	5
The narrow temperature difference of preheater (K)	$\Delta T_{\text{pp,p}}$	5
The narrow temperature difference of condenser (K)	$\Delta T_{\text{pp,l}}$	5
H-P circulating superheat (K)	$\Delta T_{\text{sup},l}$	1–10
L-P circulating superheat (K)	$\Delta T_{\text{sup},l}$	5
H-P cycle supercoiling (K)	$\Delta T_{\text{sup},h}$	0
L-P cycle undercooling (K)	$\Delta T_{\text{sup},l}$	0
Isentropic efficiency of expander (%)	η_{i}	85
Mechanical efficiency of expander (%)	η_{e}	95
Pump isentropic efficiency (%)	η_{p}	85
The environment temperature (K)	T_0	288

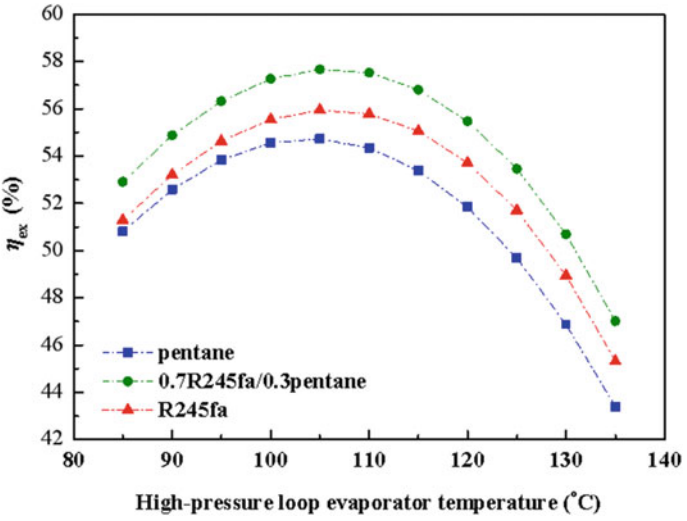

Fig. 12.3 Variations of exergy efficiency with HT-Loop evaporation temperature

to the right, which reduces the mass flow of the H-P circulating working fluid and increases the specific enthalpy of the H-P expander. The overall enthalpy difference of the H-P expander appears first. When the increase is lower, the maximum value of the work done can be found. At the same time, the mass flow of the working fluid in the L-P cycle gradually decreases with the increase of the evaporation temperature. The total working fluid flow decreases first and then increases, and the work of the L-P expander decreases and then increases, but the change is less than for the H-P expander. In theoretical analysis, the power loss of the working fluid pump is negligible relative to the work performed by the expander, so the net output work increases first and then decreases with the rise of H-P evaporation temperature. On the other hand, as the evaporation temperature of the H-P cycle increases, the temperature of the heat source at the outlet of the H-P evaporator rises, and the radon loss of the H-P evaporator decreases, while the radon loss of the L-P evaporator decreases with the mass flow of the L-P refrigerant and the inlet temperature. The temperature of the system gradually increases and gradually becomes the dominant factor of radon loss. Therefore, the total radon loss of the system decreases first and then increases, and finally, the radon efficiency increases first and then decreases. It can also be found in the figure that the radon efficiency of the mixed working fluid is better than that of the pure working fluid, and the radon efficiency under the pentane is the lowest. It is because the existence of the slip temperature that reduces the temperature difference between the cold and heat sources in the heat exchanger. When the H-T cycle evaporation temperature reaches 105 °C, the radon efficiencies of 0.7R245fa/0.3pentane, R245fa, and pentane are 57.67%, 55.94%, and 54.73%, respectively. From the perspective of tritium analysis, it can be known that the STORC system can have better thermal performance using mixed working fluids.

Figure 12.4 shows the relationship between LEC and evaporation temperature under different working media. LEC shows a trend of decreasing first and then increased gradually, and there is a minimum point. This is mainly because when the H-T circulation evaporation temperature rises, the logarithmic average temperature difference of the H-P evaporator decreases and the investment cost increases accordingly. The investment cost of the generator is positively related to the respective output work. The investment cost of the H-P evaporator is increasingly affected by the evaporation temperature. In the end, the LEC decreases first and then gradually increases. The LEC under R245fa is always lower than the other two working fluids, indicating that the economic performance under this working condition which is best followed by 0.7 R245fa/0.3 pentane. When the H-T circulation evaporation temperature is 105 °C, the LEC of R245fa can reach a minimum of 20.26×10^{-2} \$/kWh, and at the same evaporation temperature, the minimum LEC of pentane is 21.63×10^{-2} \$/kWh; and the H-P circulation evaporation temperature is 110 °C, the LEC of R245fa/pentane can reach a minimum of 21.18×10^{-2} \$/kWh. It can be found that the economic performance of the system under pure working medium is better than that under mixed working medium.

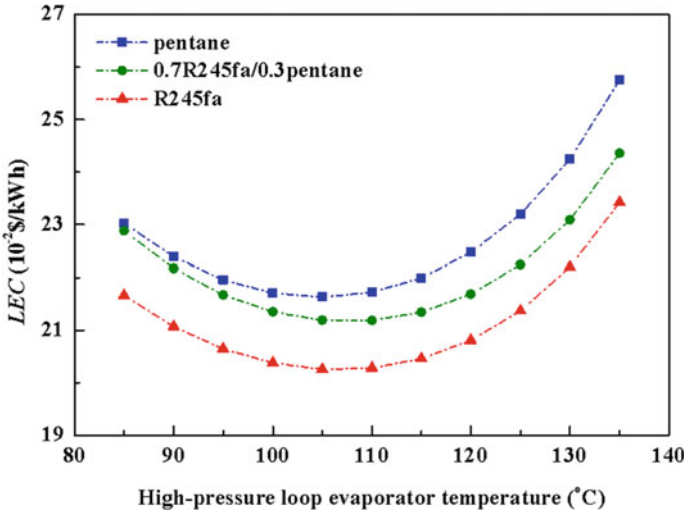

Fig. 12.4 Variations of LEC with HT-Loop evaporation temperature

12.2.2.3 Effect of H-T Cycle Superheat and Pinch Point Temperature Difference on System Performance

Figure 12.5 shows the changes in the efficiency of three kinds of working fluids with the H-T cycle superheat and the pinch point temperature difference. The radon efficiencies, superheating degree, and pinch point temperature difference of the three working fluids maintained opposite trends. This is because when the superheat degree rises, the mass flow of the working fluid decreases, so that the work decreases, and

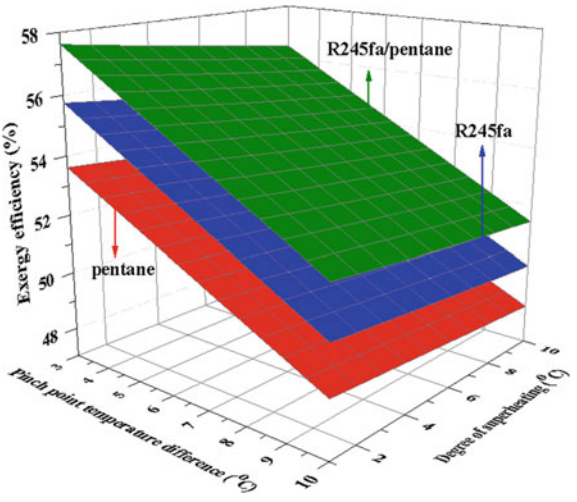

Fig. 12.5 Relationship between exergy efficiency with HT-Loop superheating degree and pinch point temperature difference

due to the power consumption of the pump which is ignored, so the net output work is continuously reduced. At the same time, we can find that the total loss of the H-P evaporator increases. Eventually, the efficiency of the loss of the H-P evaporator decreases. On the other hand, as the temperature difference at the pinch point increases, the mass flow of the working fluid decreases, resulting in a reduction in the net output power. At the same time, the total loss of the system is increasing, which is mainly due to the increase of the loss caused by the rise in the temperature of the heat source at the inlet of the L-P evaporator, so the efficiency of the loss is decreasing. Under the same superheat degree and pinch point temperature difference, the radon efficiency of R245fa/pentane is better than that of R245fa and pentane, indicating that the thermal performance of pentane is the worst. When the superheat degree is 1 K and the pinch point temperature difference is 3 K, the pentane, 0.7R245fa/0.3pentane, and R245fa can reach the maximum efficiency of 53.62%, 57.63%, and 55.75%.

The change of the LEC of the system with the superheat degree of the H-P cycle and the pinch point temperature difference is shown in Fig. 12.6. It can be seen that the LEC and the H-T cycle superheat degree and the pinch point temperature difference, all have a positive correlation. When H-P cycle superheat is increased, the work done by the high and L-P expanders decreases, which reduces the investment cost. The investment cost of the L-P evaporator also reduces the heat exchange area, although the investment cost of the H-P evaporator has increased. However, the total investment cost has been reduced, and under the combined effect of investment costs and output power, the LEC and superheat degree remain the same trend. The LEC increases with the increase of the temperature difference at the pinch point. The LEC under R245fa/pentane is between two pure working fluids, which means that the best economic performance may not be obtained with mixed working fluids. At the same time, the LEC under R245fa is the lowest and the economic performance is the best,

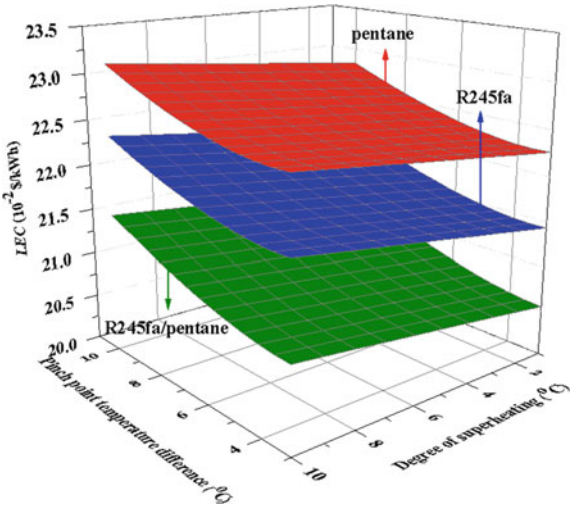

Fig. 12.6 Variations of LEC with HT-Loop superheating degree and pinch point temperature difference

while the pentane has the highest LEC and the economic performance worst. When the superheat is 1 °C and the pinch point temperature difference is 3 °C, the LECs of pentane, 0.7R245fa/0.3pentane and R245fa can reach the lowest values of 22.26 $\times$ 10^{-2} \$/kWh, 21.44 $\times$ 10^{-2} \$/kWh, and 15.50 $\times$ 10^{-2} \$/kWh, respectively.

12.2.3 Thermo-economical Optimization of STORC

In this section, the non-dominated genetic algorithm (NSGA-II) is used to optimize the STORC system for two goals. In order to consider the thermal performance and economic performance of the system, efficiency and LEC were chosen as the objective functions. At the same time, five mass fractions of R245fa, evaporation temperature of H-P cycle, pinch point temperature difference, superheat, evaporation temperature, and condensation temperature of the L-P cycle were selected as the decision variables, and the operating parameters are given in Table 12.2. Genetic algorithm parameter settings are that genetic scale is 100, genetic generation is 200, crossover factor is 0.8, and mutation factor is 0.2. Its Pareto optimal front is shown in Fig. 12.7. Efficiency and LEC maintain the opposite trend. The LEC at point A is 20.10 $\times$ 10^{-2} \$/kWh, and the efficiency is 59.01%, which indicates the best economic performance under point A, and the thermal performance is the worst. The efficiency at point B is 61.39%, and the LEC is 21.91 $\times$ 10^{-2} \$/kWh, which means that the system has the best thermal performance under the condition of point B. The system cannot reach the ideal state in which the highest chirp efficiency and the lowest LEC coexist. On the other hand, the range of variation of the unitary efficiency and LEC is small, which indicates that the system's optimal unitary efficiency and the corresponding operating parameters under the minimum LEC are close.

The solutions of the Pareto optimal front can be used as final results, and the relative order of the Pareto optimal front solutions can be determined according to different decision-making methods. Commonly used decision methods are TOPSIS

Table 12.2 Two-objective optimization results for mixture working fluid

Design parameters	A	B	TOPSIS	LINMAP	Shannon
E_{sys}(%)	59.01	61.39	60.10	60.32	59.07
LEC (10^{-2} \$/kWh)	21.91	20.10	20.41	20.48	20.11
$T_{eva,h}$ (°C)	116.70	114.24	114.58	114.25	116.69
$T_{eva,l}$ (°C)	76.06	76.79	76.85	76.67	76.14
T_{con} (°C)	30.00	30.00	30.00	30.01	30.00
$\Delta T_{sup,h}$ (°C)	3.74	4.26	4.10	4.00	3.74
$\Delta T_{pp,h}$ (°C)	5.07	4.07	4.24	4.08	4.96
r_{245fa}	0.85	0.62	0.77	0.76	0.85

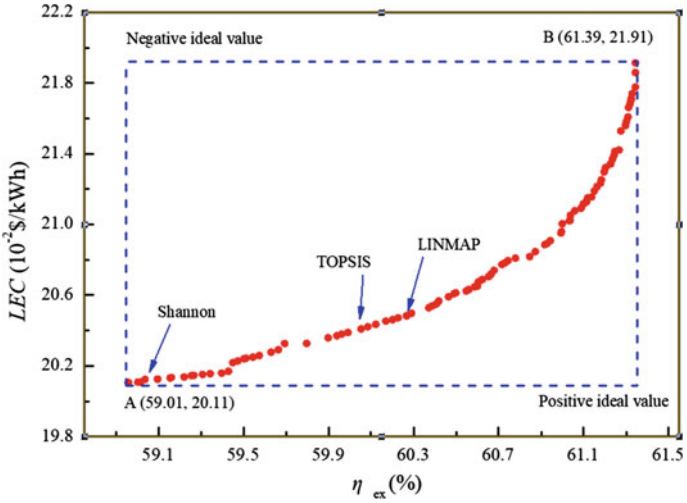

Fig. 12.7 Pareto frontier solution for two-objective optimization

(distance decision of pros and cons), LINMAP (multidimensional preference analysis linear programming decision), and Shannon (entropy decision). Among them, TOPSIS and LINMAP determine the order of the frontier solutions by determining the distance between the frontier solution and the ideal solution by different rules, and Shannon decision can be used to evaluate the system by combining the gray correlation method (GRA) to calculate the gray correlation between the frontier solution and the ideal solution. This section uses these three decisions to solve the optimal solution.

The TOPSIS decision first calculates the distance between each sample and the positive ideal solution and the negative ideal solution and then finds the relative closeness to the positive ideal solution. The greater the relative closeness, the higher the degree of matching with the ideal solution, the better the evaluation result. In the TOPSIS decision, the relative closeness of the individuals in the Pareto front solution is 0.733, 60.10% and 20.41×10^{-2} \$/kWh.

After calculating the distance of ideal solution from Euclidean distance, first, calculate the distance between each sample and the positive ideal solution and the negative ideal solution. And then find the distance to the positive ideal solution. The boundary solution with the smallest distance can be used as the final solution. The distance between the individual and the ideal solution in the Pareto front solution set in the LINMAP decision that the best advantage appears at point 53 with a distance of 0.0025. The corresponding Pareto solution has a martingale efficiency and a LEC of 60.32% and 20.48×10^{-2} \$/kWh, respectively.

Shannon and GRA decision making first calculate the weighting factors of the optimization objects according to the Shannon method, which intuitively represents the relative importance of the optimization objects. Then through GRA, the correlation coefficient between each Pareto frontal solution and the ideal solution is obtained

to obtain the gray correlation value. The larger the gray correlation value, the more the solution and the ideal solution match, so the final solution can be determined based on the gray correlation value. The gray correlation value of the frontier solution and the ideal solution in the Shannon and GRA decision that the best advantage is at point 81 and the gray correlation is 0.761. The Pareto solution corresponds to a martingale efficiency and a LEC of 59.07% and 20.11 $\times$ 10^{-2} \$/kWh.

12.2.4 Thermo-environmental Optimization of STORC

By efficiency and LEC double objective optimization, which can be concluded that the thermal performance and economic performance of operation parameters, including working fluid the best mix proportion is 0.77/0.23, because of the working fluid under different mixing proportion of equivalent coefficient of carbon dioxide emissions to the environment impact of indicators of ECE difference. This section will be used only for 0.23 pentane/0.77 R245fa as working fluid, STORC system further optimized, in search of both systems operating conditions of thermal environment performance. Exergic efficiency, LEC, and environmental ECE were selected as the objective functions. H-P cyclic evaporation temperature, superheat and pinch temperature difference, L-P cyclic evaporation temperature, and cold and warm temperature were selected as the decision variables. Genetic algorithm parameter settings are that the genetic scale is 120, the genetic algebra is 300, the crossover factor is 0.8, and the variance factor is 0.2. The optimal Pareto front is shown in Fig. 12.8.

The two-dimensional diagram of Pareto is shown in Fig. 12.9 to better reveal the relationship of the objective function. It can be found that the lowest ECE at point C (57.98%, 20.81 $\times$ 10^{-2} \$/kWh, 9.25 $kgCO_2eq/kWh$) indicates the optimal system environmental performance under this working condition, while exergic efficiency and thermodynamic performance are the worst. Meanwhile, the low LEC indicates optimal economic performance. Exergic efficiency was the highest at E point (62.11%, 21.06 $\times$ 10^{-2} \$/kWh, 9.54 $kgCO_2eq/kWh$), while both LEC and ECE reached the maximum value, indicating that economic performance and environmental performance were decreasing while thermal performance was improved. The LEC at point D (59.17%, 20.66 $\times$ 10^{-2} \$/kWh, 9.27 $kgCO_2eq/kWh$) was the lowest, indicating that the economic performance was the best under the working condition of this point. Both ECE and exergic efficiency were in low positions, indicating that the environmental performance was better, while the thermal performance was poor. Table 12.3 lists the points C, D, and F, as well as the values of the objective function and running parameters under the optimal solution after the decision by TOPSIS, LINMAP, and Shannon. Further calculations show that the migration factors of the optimal solution under the three decisions are 0.283, 0.288, and 0.541, respectively. TOPSIS decision points are selected as the final solution.

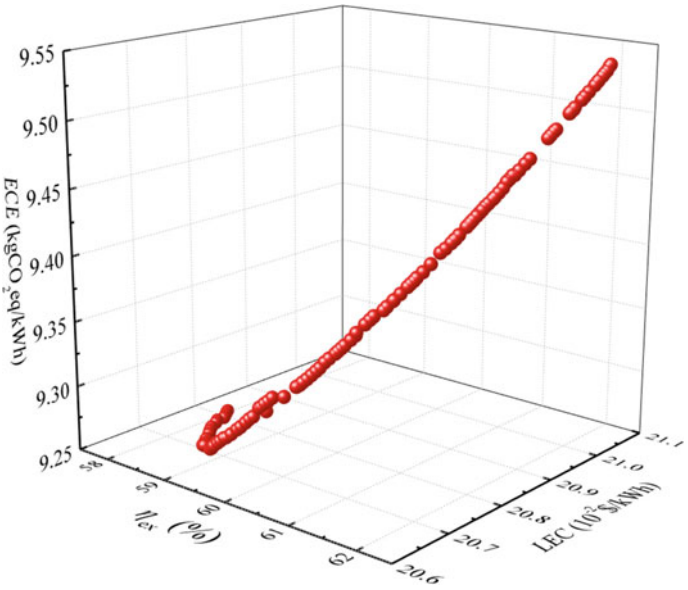

Fig. 12.8 Pareto frontier solution for three-objective optimization

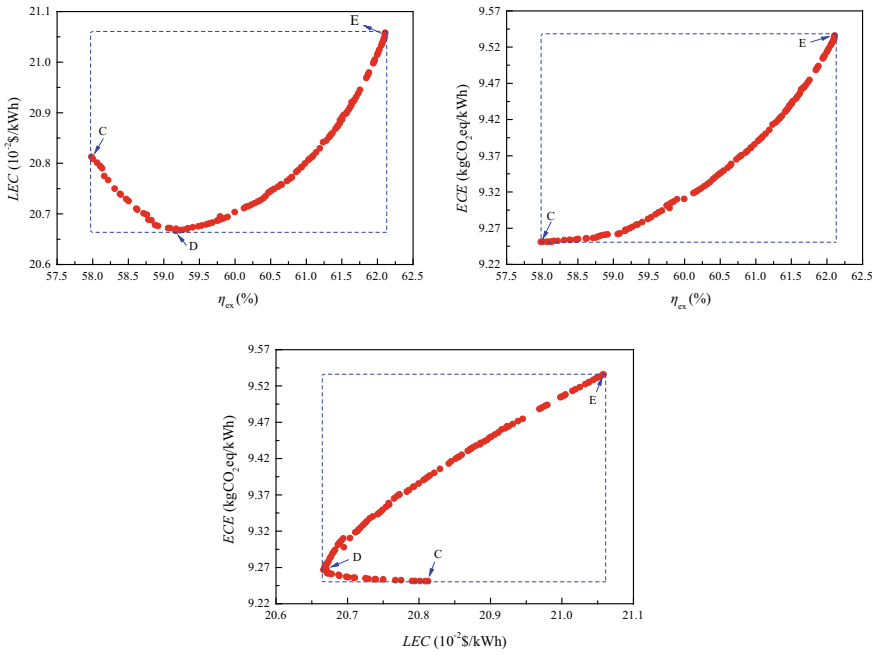

Fig. 12.9 2D graph of Pareto frontier solution for three-objective optimization

Table 12.3 Three-objective optimization results

Parameters	C	D	F	TOPSIS	LINMAP	Shannon
E_{sys} (%)	57.98	59.17	62.11	61.37	61.62	59.16
LEC (10^{-2} \$/kWh)	20.81	20.66	21.06	20.86	20.91	20.67
ECE ($kgCO_2eq/kWh$)	9.25	9.27	9.54	9.43	9.46	9.27
$T_{eva,\ h}$ (°C)	122.45	113.94	116.89	117.48	117.52	114.08
$T_{eva,l}$ (°C)	78.40	79.34	80.00	80.00	79.99	79.31
T_{con} (°C)	30.00	30.00	30.00	30.00	30.00	30.00
$\Delta T_{sup,h}$ (°C)	1.01	1.00	1.00	1.00	1.00	1.00
$\Delta T_{pp,h}$ (°C)	10.00	10.00	3.00	4.66	4.10	10.00

12.3 Thermo-environmental Optimization of a Cascaded Organic Rankine Cycle (CORC) Using Mixture Working Fluids

12.3.1 System Description

As illustrated in Fig. 12.10, the CORC includes a HT-Loop ORC and a LT-Loop (L–T loop) ORC. The HT-Loop is composed of a pump (pump-1), two evaporators

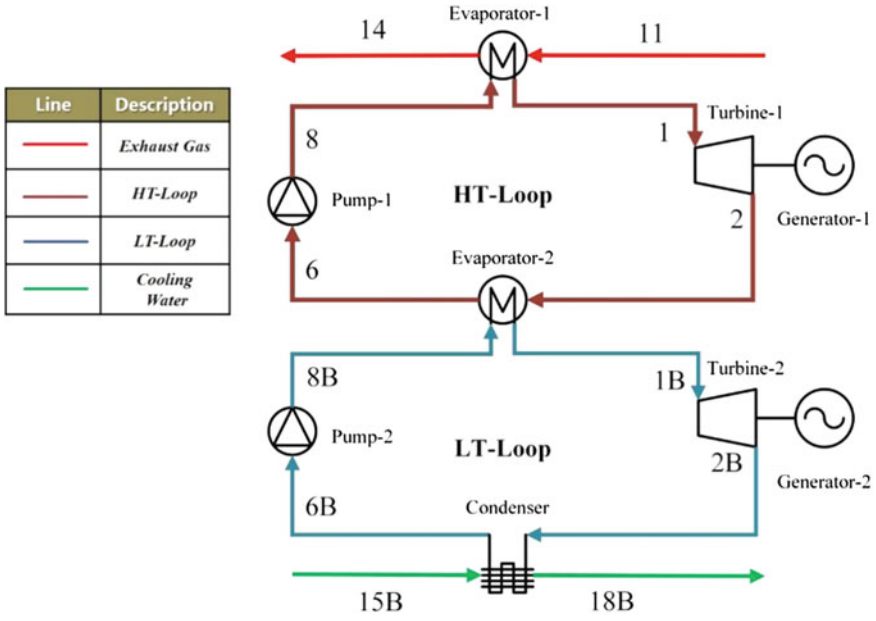

Fig. 12.10 Schematic diagram of the CORC system for L–T waste heat

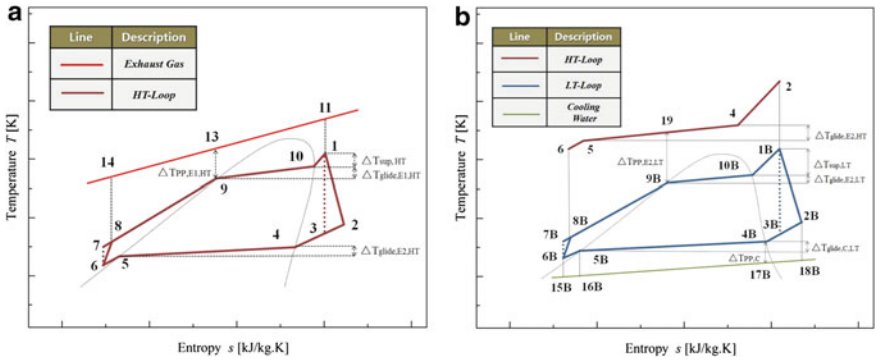

Fig. 12.11 **a** *T-s* diagram of the HT-Loop. **b** *T-s* diagram of the LT-Loop using mixture working fluid

(evparotor-1 and evaporator-2), a turbine (turbine-1), and a pump (pump-1), while the LT-Loop owns a turbine (turbine-2), a pump (pump-2), and a condenser (condenser). It should be noted that the evaporator (evaporator-2) for LT-Loop acts as condenser for HT-Loop.

In HT-Loop, the exhaust gas heated up the working fluid and that working fluid is evaporated in the evaporator-1 and then enters the expander-1 for work. After doing work, the waste steam enters the evaporator-2 and exchanges heat with the LT-Loop working fluid-2. Finally, working fluid is entered in the evaporator-1 by pump for the next HT-Loop. LT-Loop performs a cycle like the HT-Loop, but the heat from HT-Loop.

The key advantage of using mixture working fluid is that pure working fluids can better match the heat sink and heat source. Figure 12.11 shows the corresponding *T-s* diagram of CORC system by using working fluid mixture.

12.3.2 Selection of Working Fluids

The primary criteria of selection of working fluid for the HT-Loop is the high decomposition temperature, representing that it can exert in H-T working condition. Meanwhile, it presents a high boiling temperature at atmospheric pressure to easily convert the heat in working fluids into the LT-Loop with only regular condensing pressures. As to the LT-Loop, the critical temperatures of working fluids take precedence. Meanwhile, R245fa/R227ea, R245fa/R600a, R245fa/pentane, and R245fa/R152a were commonly used to compare with the pure working fluids. R11 and R123 were suggested as the flame retardants for waste heat recovery using mixing with cyclohexane, cyclopentane, and benzene. Therefore, Cyclohexane/R11 is chosen as the HT-Loop working fluid, while those four working fluid mixtures

Table 12.4 Physical properties of working medium

No.	Working fluids	M (kg kmol^{-1})	T_{cr} (K)	P_{cr} (MPa)	$T_{boiling}$ (K)
1	Cyclohexane	84.161	553.64	4.07	353.89
2	R11	137.37	471.11	4.41	296.86
3	R245fa	134.05	427.05	3.65	288.29
4	R227ea	170.03	374.90	2.93	256.81
5	R600a	58.122	407.81	3.63	261.40
6	R152a	66.051	386.41	4.51	249.13
7	Pentane	86.175	507.82	3.03	341.86

(R245fa/R600a, R245fa/R227ea, R245fa/pentane, and R245fa/R152a) are considered as research object for LT-Loop. The detailed thermophysical properties of five nominated mixture working fluids are illustrated in Table 12.4.

12.3.3 Multi-objective Optimization

12.3.3.1 Objective Functions and Decision Variables

This study explores thermal economy optimization and thermal optimization for exergy efficiency maximization and LEC minimization. At the same time, the seven system parameters, which includes outlet temperature of evaporator of HT-Loop, condenser temperature of HT-Loop, degree of superheat of HT-Loop, pinch point temperature difference, outlet temperature of evaporator, condenser temperature of LT-Loop, and the mass fraction of R245fa are chose as the decision variables. The list of these constraints is presented in Table 12.5.

In order to examine the effects of operation parameters on system performance, 0.75 Cyclohexane/0.25 R11 is selected for HT-Loop, while four mixture working fluids are chosen for LT-Loop. The effects of six operation parameters (outlet temperature of evaporator of HT-Loop, condenser temperature, pinch point temperature difference of HT-Loop, degree of superheat, outlet temperature of evaporator of LT-Loop, and condenser temperature).

The operational parameters of HT-Loop and LT-Loop have a noteworthy effect on the system's behavior. Meanwhile, the mass fraction of mixture working fluid affects the temperature glide, thereby influencing the match between the heat source/heat sink and the working fluid. Therefore, the parametric analysis on the exergy efficiency and LEC is conducted at first. It should be renowned that the working fluid mixtures with a constant mass fraction are adopted for parametric analysis due to the similar phenomenon which can be obtained for the working fluid mixtures with the other mass fractions.

Table 12.5 Main assumptions for the CORC system

Item	Unit	Value
Heat sources temperature	K	573
Expander isentropic efficiency	[%]	80
Generator efficiency	[%]	90
Pump isentropic efficiency	[%]	80
Pump efficiency	[%]	90
Mass flow of heat sources	kg s^{-1}	0.33
Cooling water temperature	K	283
HT-Loop evaporator outlet temperature	K	513
LT-Loop evaporator outlet temperature	K	333
HT-Loop degree of superheat	K	5
LT-Loop degree of superheat	K	5
Pinch point temperature difference in evaporator-1	K	6
Pinch point temperature difference in condenser	K	5
HT-Loop condenser temperature	K	413
LT-Loop condenser temperature	K	308
Environmental temperature	K	293

12.3.3.2 Effect of Parameters of HT-Loop on Exergy Efficiency and LEC

The relationship between exergy-efficiency, outlet temperature of evaporator of HT-Loop, and condenser temperature of HT-Loop using working fluid mixtures is shown in Fig. 12.12. The HT-Loop evaporator outlet temperature increases from 463 to 513 K, while the HT-Loop condenser temperature increases from 403 to 413 K. Obviously, for those four different working fluid mixtures, a better exergy efficiency is yielded with a higher evaporator outlet temperature or a higher HT-Loop condenser temperature. What should be emphasized that the condenser of HT-Loop acts as an evaporator for the LT-Loop.

As can be seen from the picture, when the outlet temperature of evaporator of HT-Loop keeps rising, the difference of specific enthalpy goes up, whereas the mass flow rate yields a reverse trend. The increasing difference of specific enthalpy is predominant than that of the decreasing mass flow rate, which results the net-power output increase. Meanwhile, with the increase of the evaporator outlet temperature (exergy), failure shows the same trend. Moreover, rising outlet temperature of evaporator of HT-Loop causes a decline in net-power output, and so the exergy efficiency goes down. Among those four working fluid mixtures, 0.5R245fa/0.5R227ea obtains the highest value of exergy efficiency.

The variation of LEC with outlet temperature of evaporator of HT-Loop and condenser temperature of HT-Loop by using working fluid mixtures is illustrated in

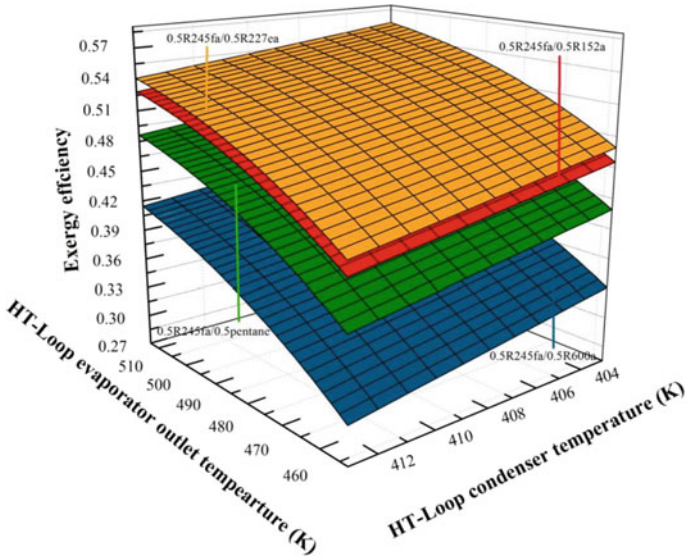

Fig. 12.12 Relationship between exergy efficiency, HT-Loop evaporator outlet temperature, and condenser temperature using mixture working fluids

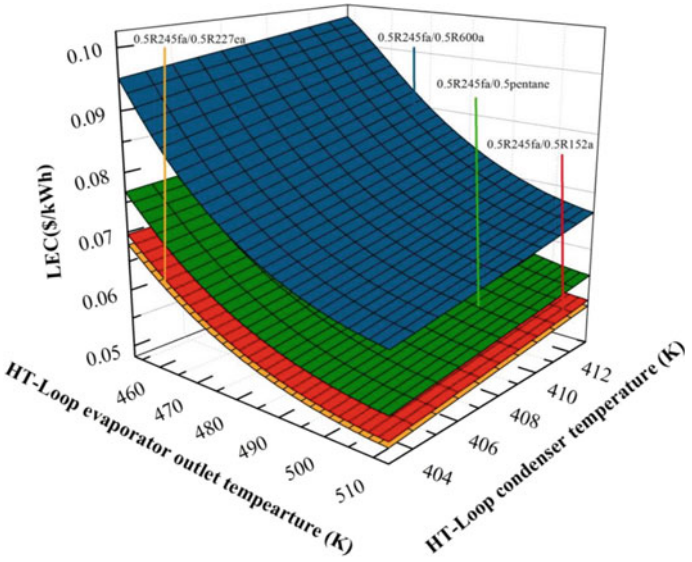

Fig. 12.13 Variation of LEC with HT-Loop evaporator outlet temperature and condenser temperature using mixture working fluids

Fig. 12.13. The LEC of the mixture of the four working media increases with the increase of the temperature of the condenser in the H-T circuit.

The rising outlet temperature of evaporator of HT-Loop decreases the area of heat transfer, resulting in a decline of investment cost in the system. The influence of the descending investment cost of the system and the ascending net-power output comprehensively leads to the descending in LEC at first. With the further rise of outlet temperature of evaporator of HT-Loop, the descending net-power output turns out slowly significant, and thus, the decline of LEC is gradually slowing. Moreover, the increasing condenser temperature of HT-Loop keeps the difference of mean heat-transfer temperature in condensing section of condenser to ascends, causing a decrease in the area of heat transfer of condenser and a decline in the investment cost of the system. However, the influence of the decline of net-power output would outperform that of the decline of system investment cost. Therefore, a rising trend of LEC can be seen with the HT-Loop condenser temperature. 0.5R245fa/0.5R600a yields the highest LEC, followed by 0.5R245fa/0.5pentane, 0.5R245fa/0.5R152a, and 0.5R245fa/0.5R227ea which has the lowest LEC.

12.3.3.3 Thermo-economical Optimization of Maximizing Exergy Efficiency and Minimizing LEC

In order to obtain the optimal operation parameters, it is necessary to carry out dual-objective optimization. Meanwhile, seven operation parameters (outlet temperature of evaporator of HT-Loop, condenser temperature of HT-Loop, pinch point temperature difference of HT-Loop, degree of superheat of HT-Loop, outlet temperature of evaporator of LT-Loop, condenser temperature of LT-Loop, and mass fraction of R245fa) are chosen as the decision variables. The lower bound and upper bound of those seven decision variables are listed in Table 12.6. The parameters of genetic algorithm including generation size, population size, crossover fraction, and migration fraction are set to 100, 60, 0.8, and 0.2, respectively.

The Pareto optimal frontiers of LEC for working fluid mixtures are demonstrated in Fig. 12.14. Obviously, a distinct trade-off can be found between thermodynamic

Table 12.6 Data of the parameter optimization

Decision variables	Lower bound	Upper bound
HT-Loop evaporator outlet temperature (K)	453	513
LT-Loop evaporator outlet temperature (K)	333	363
HT-Loop condenser temperature (K)	403	413
LT-Loop condenser temperature (K)	303	313
HT-Loop pinch point temperature difference (K)	6	12
HT-Loop degree of superheat (K)	2	5
Mass fraction of R245fa	0.1	0.9

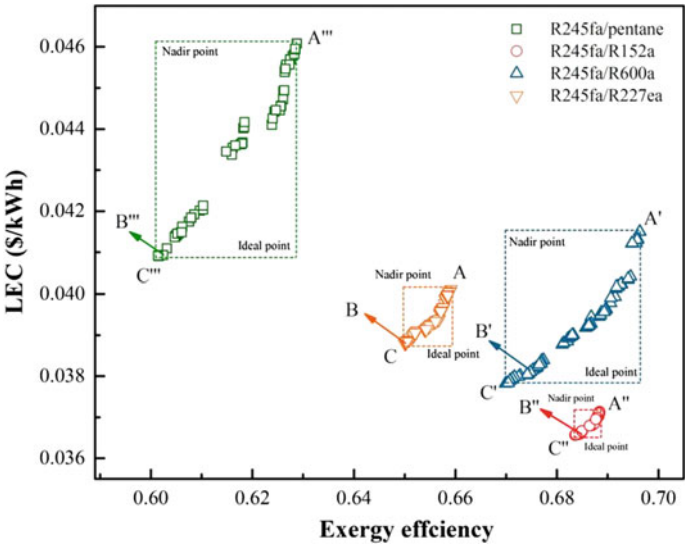

Fig. 12.14 Pareto optimal frontiers of LEC with exergy efficiency using mixture working fluid

and economic performance. As exergy efficiency increases, the LEC starts to ascend slightly at first and then a sharp increase. Taking R245fa/R227ea as an example, the highest thermodynamic performance, which is represented by point A, is 65.91% in exergy-efficiency, but holds the highest economic performance at the same time (0.04 $/kWh for LEC). Meanwhile, the optimal point cannot satisfy both of exergy efficiency and LEC which are optimal, so the TOPSIS decision making is used to get the Pareto optimal solution. The optimal point is illustrated in Fig. 12.14 with the point of B for R245fa/R227ea. It should be mentioned that point A presents the optimum thermodynamic performance, which is obtained by single-objective optimization of maximizing exergy efficiency, while point C presents the optimum economic factors, owning by single-objective optimization of minimizing LEC.

A hypothetical point, which denotes the ideal point, is considered as the best solution to get the optimal point. The ideal point is situated at lower right. From the viewpoint of thermo-economic optimization, a working fluid with Pareto optimal frontier solution located at lower right should take precedence. As observed in Fig. 12.14, R245fa/R152a is the nearest working fluid to the ideal point, while R245fa/pentane is the nearest working fluid to the nadir point. It demonstrates that R245fa/R152a is the best candidate working fluids for CORC LT-Loop.

According to the objective optimization of exergy efficiency, R245fa/R600a has the highest exergy efficiency of 69.63%, which is 5.64% higher than R245fa/R227ea, 1.15% higher than R245fa/R152a, and 10.72% higher than R245fa/pentane. Through the single-objective optimization of LEC, the lowest LEC of 0.036 $/kW h is yielded for R245fa/R152a, which is 5.26% lower than R245fa/R227ea, 5.26% lower than

R245fa/R600a, and 12.19% lower than R245fa/pentane. Meanwhile, the optimum mass fraction is ranging from 38.93 to 69.92%.

12.3.3.4 Thermo-environmental Optimization of Exergy Efficiency, LEC, and Minimizing SEI

Although thermal economy optimization improves system performance, but it not considers the environmental factor. Taking the SEI into account, the tri-objective optimization of maximizing exergy efficiency, minimizing LEC, and minimizing SEI is addressed. It should be noted that those seven operation parameters are selected as decision variables, while maximizing exergy efficiency, minimizing LEC, and minimizing SEI are considered simultaneously. The Pareto optimal frontiers for thermo-environmental optimization mixture using working fluids are displayed in Fig. 12.15. The Pareto optimal solution can be obtained based on the TOPSIS decision making.

Pareto optimal solution of four mixed working media are the points A, B, C, and D, respectively. Pareto optimal solutions for R245fa/R227ea, R245fa/R600a, R245fa/R152a, and R245fa/pentane in pairs of (LEC ($/kWh), exergy efficiency (%), and SEI (kg CO_2eq/m^2)) are (0.038, 65.24, 0.498), (0.036, 69.75, 0.415), (0.037,

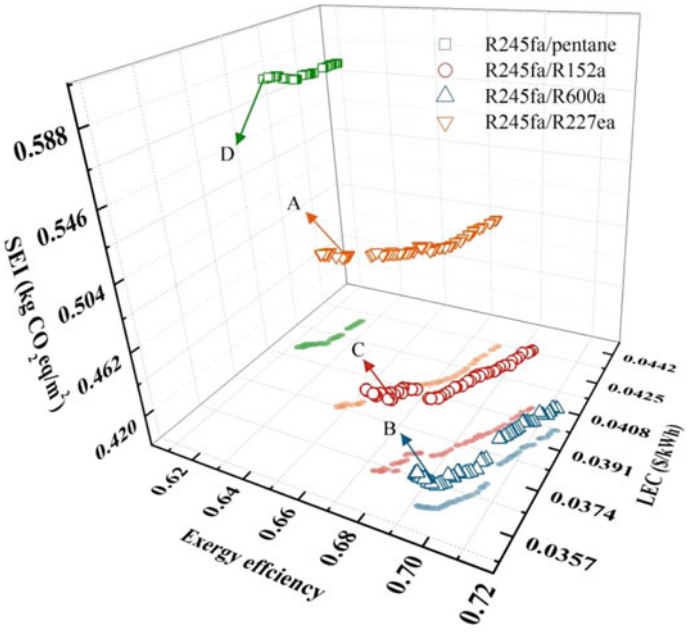

Fig. 12.15 Pareto optimal frontiers for thermo-environmental optimization mixture using working fluids

67.98, 0.446), and (0.041, 61.28, 0.584), respectively. The mass fraction is ranging from 41.64 to 89.11%.

12.4 Experimental Investigation of Heat Exchanger Characteristics on a 3 kW ORC

12.4.1 Experimental Setup Description

As shown in Fig. 12.16, a 3 kW ORC experimental unit is build. The process includes three sub-cycles. The first cycle is the ORC loop, which is the main loop. The cycle consists of five main components, evaporator, expander, condenser, working pump, and generator, as well as valves, pipelines, measuring and control instruments, etc. The low boiling working fluids are heated to a superheated vapor state in the evaporator. This high-pressure vapor is fed to the expander to generate work. The exhaust is cooled in the condenser. The working pump extracts the working fluid from the storage tank and pressurizes it into the evaporator, and the working fluid absorbs heat again in the evaporator. Thereby, working fluid completes the cycle of "heat absorption-work-condensation-pressurization" and simultaneously realizes the

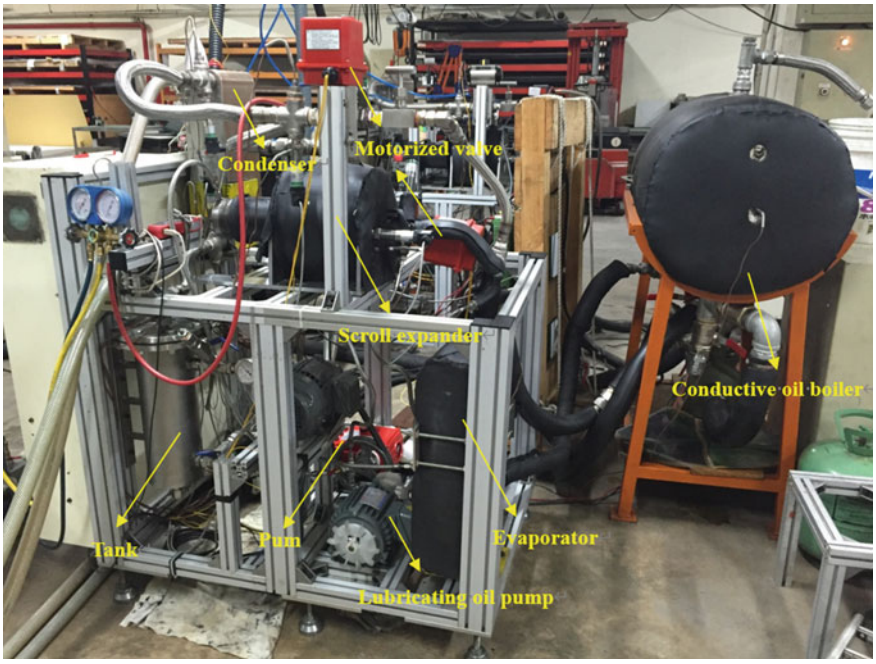

Fig. 12.16 Photograph of experimental setup

conversion process from low-grade thermal energy to high-grade electrical energy. A plunger pump is utilized as the working pump because of its high-volume ratio and small flow rate, and a scroll expander is selected. The second cycle is the heat source loop. In this experiment, the heat source is simulated by means of electric heating conductive oil, and the conductive oil enters the evaporator and transfers heat to the working fluids. The third cycle is the cooling water loop, which exchanges heat with the working fluid by cooling water.

12.4.2 Comparison of Heat Transfer Performance with Various Mass Fraction

Based on the literature review, the comparison of heat transfer coefficients between mixtures and pure working fluid were not well reported. To provide a better guide for the heat exchanger design using mixture working fluids, a detailed discussion on heat transfer performance with various mass fraction is examined in this section.

Figure 12.17 reveals the variation of the evaporator heat transfer coefficients at different R245fa mass fraction. It can be seen from the figure that there is a positive correlation between the two. This shows that R245fa is better for the heat transfer of the evaporator than the R123. R245fa has higher latent heat of evaporation than R123, so R245fa unit mass heat absorption is greater than R123. When the mass fraction of R245fa increases, the heat transfer rate with the heat source will gradually increase, and thus, the heat transfer performance of evaporator is also improved.

Meanwhile, the evaporator heat transfer coefficients are in range of 211.6–273.3 W/m^2 °C for R123, 220.8–334.3 W/m^2 °C for R24fa/R123 mixtures, and 290.6–446.4 W/m^2 °C for R245fa. The evaporator heat transfer coefficients for

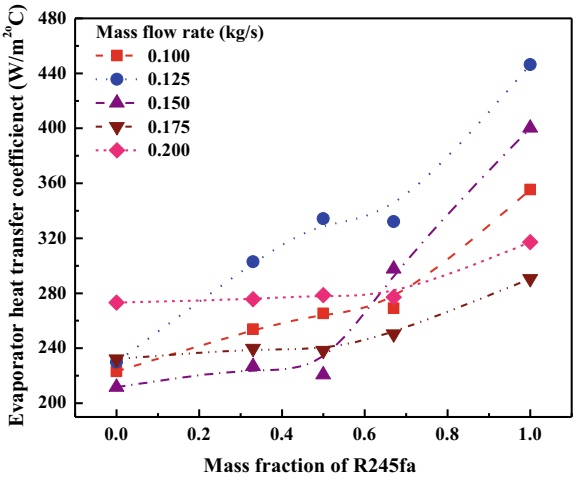

Fig. 12.17 Variation of evaporator heat transfer coefficients with mass fraction of R245fa

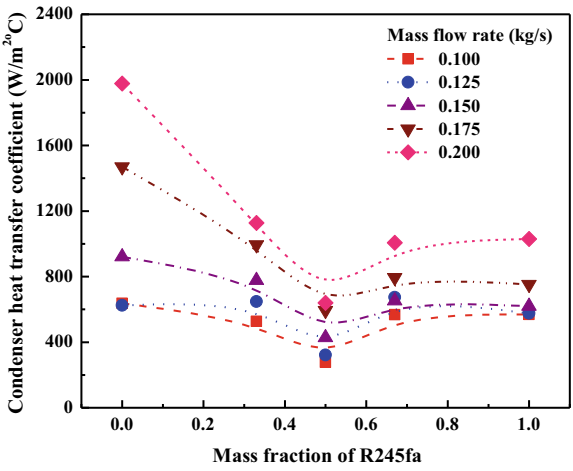

Fig. 12.18 Variation of condenser heat transfer coefficients with mass fraction of R245fa

R245fa/R123 mixtures are 1–45% higher than that for R123, but 12–45% lower than that for R245fa. Meanwhile, R245fa has 16–94% higher evaporator heat transfer coefficients than R123. It can be also found that the mass flow rate has a great effect on evaporator overall heat transfer coefficient for R245fa and R245fa/R123 mixtures, but no obvious effect for R123. The evaporator overall heat transfer coefficient presents a "N" shape trend with mass flow rate.

The variation of the condenser heat transfer coefficients is illustrated in Fig. 12.18. As can be seen from the figure, 0.5R123/0.5R245fa obtains the lowest condenser heat transfer coefficient. The condenser heat transfer coefficients are in the range of 625.3–1978.1 W/m^2 °C for R123, 277.6–1127.1 W/m^2 °C for R24fa/R123 mixtures, and 569.6–1030.0 W/m^2 °C for R245fa. The condenser heat transfer coefficients of R245fa/R123 mixtures (only for part specified mass fraction) are higher than that of R245fa, but lower than that of R123. Taking a mass flow rate of 0.200 kg/s as an example, the condenser heat transfer coefficients decrease from 1978.1 to 639.1 W/m^2 °C and then increase to 1030.0 W/m^2 °C. 0.5R123/0.5R245fa owns a worse condenser heat transfer coefficient, which is 38% lower than that of R245fa and 68% lower than that of R123.

12.4.3 Comparison Between the Experimental Test and Simulation Result Without Considering the Pressure Drop

The ORC theoretical calculation has a larger deviation with the experimental results. One reason is that the simulation ignored the pressure drop and the components' characteristics, resulting in the theoretical analysis cannot better guide the experiment prototype design. In order to ascertain the effect of pressure drop, a detailed

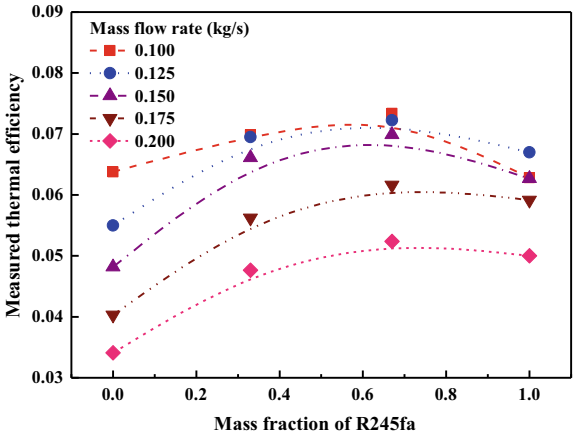

Fig. 12.19 Variation of measured thermal efficiency with mass fraction of R245fa

comparison on the thermal efficiency between the experimental test and simulation result without considering the pressure drop is addressed in this section.

The measured thermal efficiency with R245fa mass fraction is shown in Fig. 12.19. The trend in thermal efficiency indicating that an optimal mass fraction is existed to ensure the maximum thermal efficiency. The measured thermal efficiency is in range of 3.41–6.38% for R123, 4.76–7.33% for R123/R245fa mixtures, and 5.00–6.28% for R245fa. 0.67R123/0.33R245fa yields the highest measured thermal efficiency of 7.33%, which is 15% higher than R123 and 10% higher than R245fa. Meanwhile, a higher mass flow rate owns a smaller measured thermal efficiency. The reason for this is that a higher mass flow rate causes a higher system heat input and pump consumption. The mass flow rate presents insignificant effect on the measured thermal efficiency for R245fa and R123/R245fa mixtures for a mass flow rate smaller than 0.150 kg/s. However, the measured thermal efficiency for R123 has a sharp decrease from 6.38% to 3.41%. The maximum measured thermal efficiency of 0.67R123/0.33R245fa are 7.33%, 7.22%, 6.99%, 6.16%, and 5.24% while the mass flow rate varies from 0.1 to 0.2 kg/s, respectively.

The simulated thermal efficiency without considering the heat exchanger pressure drop is plotted in Fig. 12.20. As can be seen from the figure, the thermal efficiency presents a quadratic curve law with the increase of the mass fraction of R245fa. The simulated thermal efficiency is in range of 11.95–13.02% for R123, 12.86–14.55% for R123/R245fa mixtures, and 10.49–12.64% for R245fa. When the flow rate in the heat exchanger reaches 0.200 kg/s, 0.67R123/0.33R245fa yields the thermal efficiency of 14.55%, which is 13% higher than R123 and 15% higher than R245fa. Meanwhile, lower mass flow rate represents a positive effect on the simulated thermal efficiency. For a mass flow rate higher than 0.175 kg/s, it has a small influence on the simulated thermal efficiency, whereas a significant effect when it is less than 0.150 kg/s. The maximum simulated thermal efficiency of 0.67R123/0.33R245fa are 12.93%, 14.02%, 14.39%, 14.38%, and 14.55%, respectively.

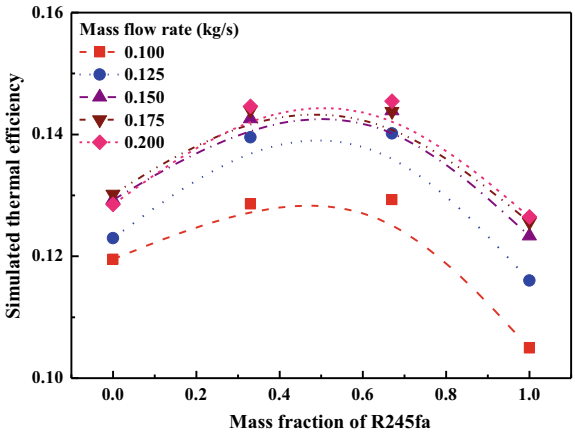

Fig. 12.20 Variation of simulated thermal efficiency with mass fraction of R245fa

To better understand the deviation between the theoretical and experimental results, the measured and simulated thermal efficiency for mass flow rate of 0.100 and 0.200 kg/s are addressed in Fig. 12.21. Obviously, with the increase of the mass fraction of R245fa, both the measured and simulated values of thermal efficiency firstly increase and then decrease. However, the increase of mass flow rate will lead to the decrease of measured thermal efficiency, whereas a reverse trend for the simulated thermal efficiency. Meanwhile, the simulated thermal efficiency is 67–277% higher than the measured one. The simulated thermal efficiency for 0.67R123/0.33R245fa has a 76% higher for mass flow rate of 0.100 kg/s and 178% higher for mass flow rate of 0.200 kg/s than the measured thermal efficiency. It demonstrates that the pressure drop of heat exchanger is significantly related to the system performance and the pressure drop of heat exchanger should be fully considered in theoretical analysis.

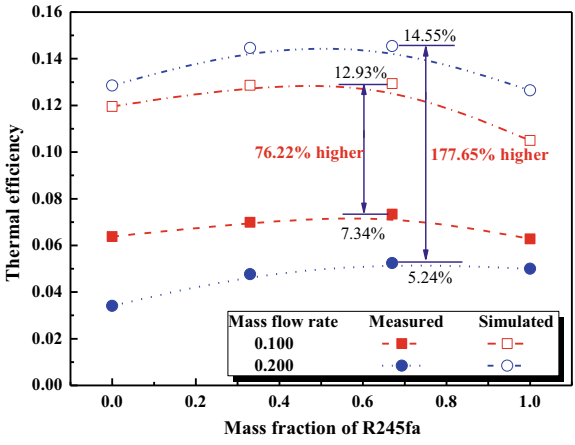

Fig. 12.21 Comparison between the measured and simulated thermal efficiency

12.5 Conclusions

Based on the thermal model and economic model of STORC system, the thermal performance of mixed working fluid R245fa/pentane and pure working fluid R245fa and pentane are understood. The effects of the six parameters including the mass ratio of the mixed working fluid, the H-P circulating evaporation temperature, the superheat, pinch point temperature difference, the L-P circulating evaporation temperature, and the condensation temperature were analyzed. Considering the thermodynamic performance, economic performance, and environmental performance simultaneously, parametric analysis and thermo-environmental optimization of a cascaded organic Rankine cycle (CORC) using mixture working fluids have been investigated. Cyclohexane/R11 is selected as working fluids for HT-Loop. The following four working fluids (R245fa/R227ea, R245fa/R600a, R245fa/R152a, and R245fa/pentane) are the candidate working fluids of the LT-Loop. The heat exchanger performance of different mixtures has been studied and compared in a 3 kW ORC experimental prototype. Five different proportions of working fluids are selected, respectively, R123, 0.33R123/0.67R245fa, 0.5R123/0.5R245fa, 0.67R123/0.33R245fa, and R245fa. The heat transfer characteristics of heat exchangers under different working fluids are studied and compared. The comparison between the experimental test and simulation result without considering the pressure drop is addressed. The main conclusions are as follows:

(1) Considering the thermodynamic performance and economic performance of the system comprehensively, selected exergy efficiency and LEC as the dual-objective optimization goals. Finally, the optimal solution under the TOPSIS decision was selected. Exergy efficiency and LEC were 60.10% and 0.2041 $/kWh, respectively. The exergy efficiency of Pareto front solution of mixed working fluid ranges from 59.01% to 61.39%, and the maximum exergy efficiency is 1.87% and 1.16% higher than Pentane and R245fa, respectively. ECE was selected as an environmental evaluation index, and the exergy efficiency, LEC, and ECE of STORC system under mixed working fluid were optimized. Finally, TOPSIS decision point (61.37%, 0.2086 $/kWh, 9.43 $kgCO_2eq/kWh$) was selected as the optimal solution.

(2) Compared with different working medium from the perspective of thermo-economic optimization, a working fluid with Pareto frontier solution located at lower right should take precedence. R245fa/R152a is the best candidate working fluids for CORC LT-Loop. According to the minimum LEC, the lowest leveled energy cost of 0.036 $/kW h is yielded for R245fa/R152a, which is 5.26% lower than R245fa/R227ea, 5.26% lower than R245fa/R600a, and 12.19% lower than R245fa/pentane. Meanwhile, the optimum mass fraction is ranging from 38.93% to 69.92%.

(3) The evaporator heat transfer coefficients of R245fa are highest, followed by the R245fa/R123 mixture and while R123 shows the lowest evaporator heat coefficients. And the condenser heat transfer coefficients of R123 are highest and that of 0.5R245fa/0.5R123 are lowest. The measured thermal efficiency

of 0.67R123/ 0.33R245fa is the highest, which is 7.33% and the maximum simulated thermal efficiency is14.55%.

Acknowledgements This work has been supported by the National Natural Science Foundation of China (51806081), the Key Research and Development Program of Jiangsu Province, China (BE2019009-4), the Natural Science Foundation of Jiangsu Province (BK20180882), the Key Research and Development Program of Zhenjiang City, China (SH2019008), the Key Project of Taizhou New Energy Research Institute, China (2018-20), and the Open Foundation Program of Key Laboratory of Wind Energy and Solar Energy Technology (Inner Mongolia University of Technology), Ministry of Education of China (2020ZD02).

References

Aziz F, Roshaan M, Man-Hoe K (2018) Exergetic and heat load optimization of H-T organic Rankine cycle. Energy Convers Manag

Campana C, Cioccolanti L, Renzi M, Caresana F (2019) Experimental analysis of a small-scale scroll expander for L-T waste heat recovery in Organic Rankine Cycle. Energy 187:115929

Dong BS, Xu GQ, Cai Y, Li HW (2014) Analysis of zeotropic mixtures used in hightemperature organic Rankine cycle. Energy Convers Manag 84:253–260

Dong BS, Xu GQ, Li TT et al (2017) Parametric analysis of organic Rankine cycle based on a radial turbine for low-grade waste heat recovery. Appli Therm Eng 126:470–479

Esra OK, Kiliç M (2020) Comparative performance analysis of ORC–VCRC combined systems based on refrigerant selection. Sci Technol Built Environ

Feng YQ, Hung TC, Zhang YN, Li BX, Yang JF, Shi Y (2015a) Performance comparison of low-grade ORCs (organic Rankine cycles) using R245fa, pentane and their mixtures based on the thermoeconomic multi-objective optimization and decision makings. Energy 93:2018–2029

Feng YF, Hung TC, Greg K, Zhang YN, Li BX, Yang JF (2015b) Thermoeconomic comparison between pure and mixture working fluids of organic Rankine cycles (ORCs) for L-T waste heat recovery. Energy Convers Manag 106:859–872

Heberle F, Preißinger M, Brüggemann D (2012) Zeotropic mixtures as working fluids in organic Rankine cycles for low-enthalpy geothermal resources. Renew Energy 37(1):364–370

Huang WC, Chang YF, Yuan YX (2019) Complementary configuration and optimal energy flow of CCHP-ORC systems using a matrix modeling approach. Complexity

Imran M, Muhammad U, Byung-Sik P, Youngmin Y (2016) Comparative assessment of organic Rankine cycle integration for L-T geothermal heat source applications. Energy

Javanshir A, Sarunac N (2017) Thermodynamic analysis of a simple organic Rankine cycle. Energy 118:85–96

Kang HS, Kim MH, Shin YH (2020) Thermodynamic modeling and performance analysis of a combined power generation system based on HT-PEMFC and ORC. Energies

Kim HR, Lee JH, Kim TS (2020) Optimal thermo-economic design of a pafc-orc combined power system. J Mech Sci Technol

Lecompte S, Ameel B, Ziviani D, van den Broek M, De Paepe M (2014) Exergy analysis of zeotropic mixtures as working fluids in organic Rankine cycles. Energy Convers Manag 85:727–739

Li S, Li WY (2018) Thermo-economic optimization of solar organic Rankine cycle based on typical solar radiation year. Energy Convers Manag

Lim TW, Choi YS, Hwang DH (2021) Optimal working fluids and economic estimation for both double stage organic Rankine cycle and added double stage organic Rankine cycle used for waste heat recovery from liquefied natural gas fueled ships. Energy Convers Manag

Meng FX, Zhang HG, Yang FB, Hou XC, Lei B, Zhang L (2017) Study of efficiency of a multistage centrifugal pump used in engine waste heat recovery application. Appl Therm Eng 110:779–786

Renno C, Petito F, Diana D (2020) Modeling of a CPV/T-ORC combined system adopted for an industrial user. Energies

Shu G, Liu L, Tian H, Wei H, Yu G (2014a) Parametric and working fluid analysis of a dual-loop organic Rankine cycle (DORC) used in engine waste heat recovery. Appl Therm Eng 113(1):1188–1198

Shu GQ, Gao YU, Tian H, Wei HQ, Liang XY (2014b) Study of mixtures based on hydrocarbons used in ORC (organic Rankine cycle) for engine waste heat recovery. Energy 74:428–438

Shu GQ, Wang X, Tian H (2016) Theoretical analysis and comparison of Rankine cycle and different organic Rankine cycles as waste heat recovery system for a large gaseous fuel internal combustion engine. Appl Therm Eng 108:525–537

Song J, Gu CW (2015) Performance analysis of a dual-loop organic Rankine cycle (ORC) system with wet steam expansion for engine waste heat recovery. Appl Eng 156:280–289

Sun QX, Wang YX, Cheng ZY, Wang JF, Zhao P, Dai YP (2020) Thermodynamic and economic optimization of a double-pressure organic Rankine cycle driven by L-T heat source. Renewable Energy 147:2822–2832

Tian H, Shu GQ, Wei HQ et al (2012) Fluids and parameters optimization for the organic Rankine cycles (ORCs) used in exhaust heat recovery of Internal Combustion Engine (ICE). Energy 47(1):125–136

Tian H, Liu LN, Shu GQ et al (2014) Theoretical research on working fluid selection for a H-T regenerative transcritical dual-loop engine organic Rankine cycle. Energy Convers Manag 86:764–773

Tian H, Chang LW, Gao YY et al (2017) Thermo-economic analysis of zeotropic mixtures based on siloxanes for engine waste heat recovery using a dual-loop organic Rankine cycle (DORC). Energy Convers Manag 136:11–26

Uusitalo A, Honkatukia J, Turunen-Saaresti T et al (2014) A thermodynamic analysis of waste heat recovery from reciprocating engine power plants by means of organic Rankine cycles. Appl Therm Eng 70(1):33–41

Wang DB, Ma YZ, Tian R et al (2018) Thermodynamic evaluation of an ORC system with a L-P Saturated Steam heat source. Energy 149:375–385

Wang Q, Wang J, Li T, Meng N (2020) Techno-economic performance of two-stage series evaporation organic Rankine cycle with dual-level heat sources. Appl Therm Eng 171, 115078 (2020)

Wang X, Shu GQ, Tian H, Wang R, Cai JW (2020) Dynamic performance comparison of different cascade waste heat recovery systems for internal combustion engine in combined cooling, heating and power. Appl Therm Eng 260:114245

Wang LB, Bu XB, Li HS (2020) Multi-objective optimization and off-design evaluation of organic Rankine cycle (ORC) for low-grade waste heat recovery. Energy

Xiao L, Wu SY, Yi TT, Liu C, Li YR (2015) Multi-objective optimization of evaporation and condensation temperatures for subcritical organic Rankine cycle. Energy 83:723–733

Xu W, Zhang JY, Zhao L, Deng S, Zhang Y (2017) Novel experimental research on the compression process in organic Rankine cycle (ORC). Energy Convers Manag 137:1–11

Yamada N, Tominaga Y, Yoshiba T (2014) Demonstration of 10-Wp micro organic Rankine cycle generator for low-grade heat recovery. Energy 78:806–813

Zhang J, Zhang HG, Yang K, Yang FB, Wang Z, Zhao GY et al (2014) Performance analysis of regenerative organic Rankine cycle (RORC) using the pure working fluid and the zeotropic mixture over the whole operating range of a diesel engine. Energy Convers Manag 84(1):282–294

Zhang XX, Zhang Y, Wang JF (2021) Evaluation and selection of dry and isentropic working fluids based on their pump performance in small-scale organic Rankine cycle. Appl Therm Eng
Zhang T, Li XP, Liu LC (2021) Thermo-economic analysis and optimization of ICE-ORC systems based on a splitter regulation. Energy
Zhou NJ, Wang XY, Chen Z et al (2013) Experimental study on organic Rankine cycle for waste heat recovery from L-T flue gas. Energy 55:216–225